A novel simulation method to evaluate the collection performance of a monolithic active pixel sensor*

FU Min(付民)[1)] TANG Zhen-An(唐祯安)[2)]

School of Electronic Science and Technology, Dalian University of Technology, Dalian 116024, China

Abstract: A novel simulation method is presented in this paper to evaluate the collection performance of monolithic active pixel sensor (MAPS) devices for minimum ionizing particle tracking. A simplified 3D matrix pixel structure is built using the computer aided design software Sentaurus. The virtual device is then divided into hundreds of parts and an independent customized X photon model is involved in each part to simulate the conditions under ^{55}Fe radiation. After data processing and analysis, charge collection efficiency, collection time and diffusion conditions can be estimated in detail. In order to verify the reliability of the method, comparisons are made between the simulations and experiments. Although there are some defects, it can be concluded that the proposed idea is a feasible method for the evaluation of the MAPS collection performance.

Key words: MAPS, charge collection, evaluation, simulation

PACS: 29.40.Gx **DOI:** 10.1088/1674-1137/35/10/010

1 Introduction

The idea of using a MAPS for the detection of ionizing radiation, in particular for high-energy charged particle tracking, was proposed by R. Turchetta in 2001 [1]. The basic pixel architecture is similar to the visible light metal oxide semiconductor (MOS) camera sensor and the readout circuits are integrated with the sensitive volume on the same wafer [2]. As the primary sensitive region, a 10–20 μm lightly doped P- epitaxial layer (epi-layer) is deposited on a heavily doped P++ substrate. When a charged particle penetrates through the detector's epi-layer, non-equilibrium electrons are generated along the track. The electrons then diffuse thermally and most of them should finally be collected by the N+ wells (see Fig. 1). A series of minimum ionizing particle MOS active pixel sensor (MIMOSA) chips have been designed, fabricated and tested successfully by Institut Pluridisciplinaire Hubert Curien (IPHC), France [3–5]. It is illustrated that the MAPS could be fabricated by a standard complementary MOS planar process, providing a low-cost, high resolution procedure for minimum ionizing particle (MIP) detection.

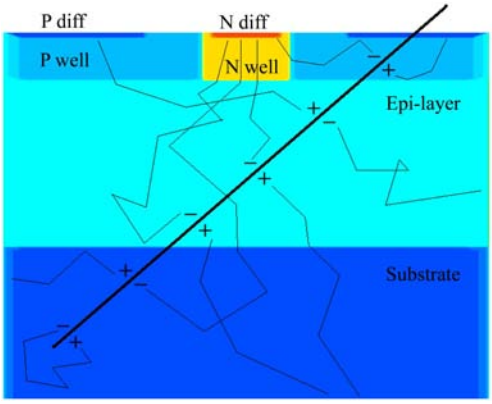

Fig. 1. (color online) The schematic cross section of a MAPS pixel. Some of the generated charges are collected by the N-well, the P-wells and the substrate, and the others are diffused and recombined.

In spite of the undeniable advantages of MAPS detectors, improvements have been made by optimizing the circuits and the detector structure. On one hand, the applications of advanced circuits such as correlated double sampling, embedded analog digital converter (ADC) and so on could improve the electri-

Received 30 December 2010

* Supported by the grant of France-China Particle Physics Laboratory (FCPPL) and China Scholarship Council (CSC)

1) E-mail: fumin1977@hotmail.com

2) E-mail: tangza@dlut.edu.cn

©2011 Chinese Physical Society and the Institute of High Energy Physics of the Chinese Academy of Sciences and the Institute of Modern Physics of the Chinese Academy of Sciences and IOP Publishing Ltd

cal performances of MAPS detectors [5, 6]. On the other hand, it is also important to optimize the pixel layout and architecture in order to collect more generated charges in less time [7]. Before the changes are realized in a real detector chip, the simulation is a compulsory procedure to find design bugs, select design parameters and estimate consequences. Furthermore, simulations are an intuitive way for researchers to understand the detection principle and collection mechanism in depth.

Although the new generation 3D simulator has been distributed, the simulation methods are still too rough to achieve the detailed collection specification evaluation, especially the key points of the MIP detector, collection time and efficiency [8]. In most researches, a heavy-ion particle model is used to penetrate a 3D virtual detector and a number of charges would be generated along the particle track. Because the charged-particle-generated free electrons can diffuse vertically from the substrate to the epi-layer as a contribution of collection (see Fig. 1), it is possible to get a collection efficiency of more than 100% if the generated charges in the substrate are neglected. In contrast, if all charges in the virtual device are regarded as the total, the achieved value would be a meaningless low number. Hence, only the number of collected charges in a certain time can be estimated [2, 8]. In addition, as a result of the non-equilibrium electron movement from the track position to the neighboring pixels, there is no appropriate approach to assess the neighboring diffusion. Evidently, it is difficult to evaluate the collection performance comprehensively using the existing simulation method.

In this paper, a novel simulation method is proposed in order to evaluate the key factors of MAPS devices, charge collection time, efficiency and neighboring diffusion, in detail. First, two 3×3 pixel matrix 3D structures with similar baselines and different resistivity epi-layers are built for comparisons with experimental measurements. They are then divided into hundreds of silicon cubes and an independent customized X photon model is involved in each cube to simulate the conditions under ^{55}Fe radiation. As in a real experiment, all output signals are collected, processed and counted after a series of physical level device simulations in transient mode. Consequently, some spectrum-like figures, charge collection time, and efficiency levels can be achieved. Finally, comparisons are made between the simulations and experiments to verify the reliability of the evaluation. Although there are some defects it can be concluded that the method is a feasible way to evaluate the MAPS collection performance.

2 Simulations

2.1 Tools

In contrast to the widespread integrated circuit simulators, there are only a few available tools for semiconductor device simulation at the physical level. In 1969, the first 2D device simulation software used for junction field effect transistor analysis appeared [9]. A decade later, the first 3D device simulation package was published [10]. As detector fabrication has developed rapidly over the last decade, this third dimension to the simulations has become very important in understanding the detector mechanism [11]. Only in the last few years have tools become accurate enough to simulate radiation detector structures in 3D. In 2008, the previous technology computer aided design software of Integrated Systems Engineering (TCAD-ISE) was superseded by the latest-generation commercial TCAD package Sentaurus of Synopsys.

In the Sentaurus package, the new subprogram Sentaurus Structure Editor (SSE) and Sentaurus Device (SD) were developed to replace the old versions Mesh-ISE and Dessis-ISE, respectively. The SSE could be used to describe the device structure interactively and then to create grids by means of a novel embedded meshing algorithm. The SD, as a solver, could address the physical level equations and the computation results could be visualized and analyzed by costumed Tecplot and script-supported Inspect, respectively [12].

2.2 Simulated structure

In order to compare with experiment, the basic frameworks of simulated structures come from the real MIMOSA-26 chip which was designed in 2008 and delivered from the foundry early in 2009 [5]. A simplified, symmetric 3×3 matrix structure is built using the aforementioned tools. The pitch size between neighboring collection electrodes is 18.4 μm. Beneath each electrode, a 3.4×4.3×3 μm^3 wedge-like N-well is plugged into the epi-layer as a probe to gather the charged-particle-generated electrons from its adjacent region. In the pixels, all the N-wells are surrounded by P-wells to suppress neighboring diffusion and integrate the associated N-type MOS circuits (see Fig. 1). The doping concentration profiles of these wells are defined by an analytical error function.

Two epitaxial wafers, which come from the already fabricated MIMOSA-26 chips, are applied in the virtual device. One is 14 μm thick and $7\times10^{14}/\mathrm{cm}^3$ P-type doped, which is a commonly used 19 Ω·cm normal resistivity (NR) epi-layer, and the other is deposited to 15 μm and doped to $3.3\times10^{13}/\mathrm{cm}^3$ as a high resistivity (HR) epi-layer, whose resistivity is 400 Ω·cm, higher than the previous one. The use of different epi-layers will lead to dissimilar collection specification and some reports have demonstrated that the HR detectors can present better collection performances due to their improved internal electric field distributions [13]. The comparisons can be used to verify the reliability of the simulation.

According to previous research by G. Deptuch [8] and D. Husson [14], only a 30 μm layer of substrate can contribute to the charge collection, although the wafers used to manufacture the detectors are generally more than 250 μm. In order to avoid unnecessary computation, the substrate in the simulated matrix is reduced to 30 μm.

The default boundary used in the SD solver is an ideal reflective condition (Neumann condition). In this case, all generated charges in the virtual device will be collected except those of recombined electrons and holes. This usually leads to an overestimation of efficiency due to the collection of actual diffused charges. To avoid this situation, auxiliary amounts of silicon are added around the pixels to emulate the procedure of charge diffusion. The whole volume is surrounded laterally by four additional oxide belts about 1 μm thick. At the interface between these oxide belts and the silicon bulk, a suitable recombination velocity is defined to consume the charges which should not be collected by the electrodes. It should be mentioned that the electrons should never be overconsumed by the boundary, nor reflected backwards. That means if an extremely high recombination velocity is used at the interface, the charges would be collected insufficiently.

2.3 Physics models

It is well known that the primary mechanism in the collection is drift and diffusion under an external excitation. Thus, the necessary physical models for carrier transport and initial condition should be selected and defined appropriately.

The mobility of the carriers is taken into account using the default doping-dependent mobility model, in which the mobility degradation due to impurity scattering is activated. Although the external voltage of the pixel diode is only 0.7 V, the high-field saturation model is still included on account of possible internal high-field regions which might be generated by the difference in doping concentrations. Additionally, the effect of carrier-carrier scattering is supported by the Conwell-Weisskopf model based on the Choo and Fletcher's screening theory [15, 16].

The recombination of the charge carriers is another essential aspect of carrier transport. That through the deep defect levels in the gap, usually labelled as Shockley-Read-Hall (SRH) recombination, is involved. Band-to-band Auger recombination, which is a typical feature at high carrier densities, is supported in the simulation and the rate is given by the Auger model with temperature-dependent Auger coefficients [17–19]. The surface SRH recombination model is also activated at the interface between the silicon and the oxide belts.

The impact ionization of the charge carriers is included using Selberherr's model [20]. This takes into account the dependence of the ionization rates on the magnitude of the electric field. A bandgap narrowing for Jain-Roulston model is also applied to define an effective intrinsic density in the heavily doped P-type silicon [21].

The default heavy-ion particle model is always used as an excitation of transient simulation, but it cannot be used directly to estimate the collection efficiency. When a virtual charged-particle penetrates a semiconductor device, it deposits its energy by generating electron-hole pairs and creates a trail of charges along the track. The trail can be defined by the length and the transverse spatial influence, which is assumed to be symmetric about the track axis and can be described as

$$G(l,r,t)=G_{\mathrm{LET}}(l)S(r,l)T(t), \tag{1}$$

where l and r are the length and the radius of the track, $S(r,l)$ and $T(t)$, both defined as Gaussian functions, are used to describe the spatial and temporal variations of generation rate, and $G_{\mathrm{LET}}(l)$ is the linear energy transfer generation density in units of pairs/cm^3. Since G_{LET} and r can be defined as functions of position along the track, the default model can be modified to emulate X photons and then to estimate the collection efficiency. Thus, the starting point of the track can be assumed to be at the location where the photon is absorbed and converted to electron-hole pairs. The radius and the length can be set to 0.5 μm and 1 μm, respectively. The volume of generated charges is then a short cylinder and can be regarded as an approximation of a sphere where

the charge concentration is $2.087\times10^{15}/\mathrm{cm}^3$, which is derived from the 1640 electron-hole pairs generated by a 5.9 keV photon [22].

Considering the symmetry of the pixel structure and the matrix, a cuboid volume within the central pixel is defined as an event region which is only one quarter of the entire pixel structure and where the involved particles are distributed uniformly. When the particles are absorbed in the cubes, the output data can be obtained by extrapolation. This zone is separated into 20 equal sub-layers, and each sub-layer is partitioned into 16 cubes whose dimensions are 2.3 μm × 2.3 μm×2.3 μm. (see Fig. 2.) Thus there are 320 cubes and X photons in total.

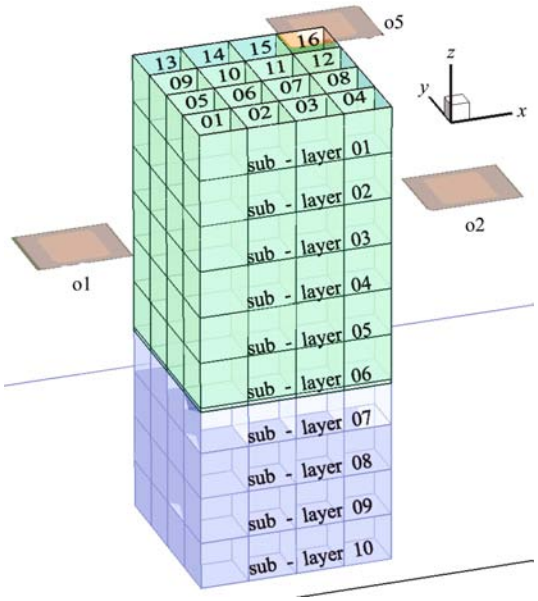

Fig. 2. Schematic of sub-layers and cubes. There are 20 sub-layers, each having 16 cubes. The bottom 10 unnecessary sub-layers are removed. o5 is the collection electrode of the central pixel.

3 Results and analysis

Before the device is solved numerically, its continuous properties should be represented by sparse meshes and defined at a finite number of discrete points in space. Graded refinements are placed in different parts of the simulated structures. The finest refinement, (0.5, 0.5, 0.5) according to the 0.5 μm grid size in the x, y and z directions, is used to mesh the central pixel. For the adjacent pixels the size is (1, 1, 1), and out of the cluster, it becomes (4, 4, 2) to simplify the meshed model. The total elements in the meshed structure are limited to half a million. Then the meshed structures are simulated in the transient mode.

The simulation output data are collected and processed using the well known analysis software Matlab. A series of figures are obtained and many details can be observed. Fig. 3 shows the total electrons collected by the matrix when the photons are injected into each sub-layer. This preliminary result illustrates that when the photons are assimilated in the bottom 10 sub-layers of the substrate, the output signals can be neglected because the charges collected by the matrix are less than the predefined threshold, which is 80 electrons in our simulations and is always determined by 6 times of noise [5]. Thus, only the data from the upper 10 sub-layers (including all the epi-layer and 8–9 μm substrate) are useful for further analysis.

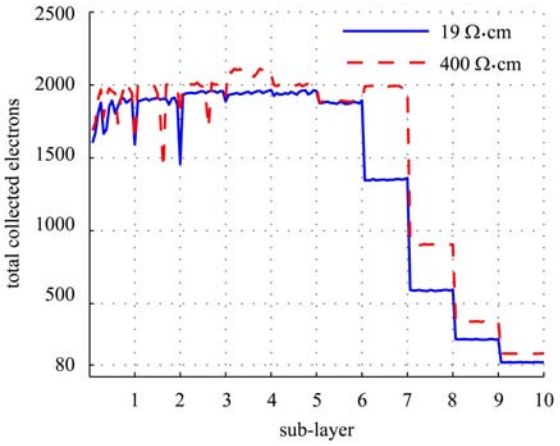

Fig. 3. Total electrons collected by each sub-layer.

In detail, the degradation of the signal in the first sub-layer demonstrates that the electrons diffuse with more difficulty in the heavily doped P-wells than in the lightly doped epi-layers. The unstable values among the sub-layers are induced by the uneven mesh grids in the entire structure. As a result of reduced contribution to the total collected charges, the output current of the sub-layers decreases step by step downwards, from the 8th sub-layer in the HR structure and from the 7th in the NR matrix. This phenomenon can be regarded as another benefit of the HR epi-layer. In addition, necessary correction operations should be performed on the diverged data for next-step analysis.

3.1 Collection efficiency

Several spectrum-like statistical curves in Fig. 4 are achieved with a 3×3 matrix cluster. For a specific view, the collection efficiencies can be fitted and extracted from the original simulation data using the

Curve Fit Tool of Matlab and then compared with the experimental results. As the max value, the 5.9 keV characteristic peak of ^{55}Fe can be regarded as the 100% point in the experiments. Accordingly, the maximum of the collected electrons should be 1640 electrons as mentioned above. The primary peaks stand for the normal collection situation. When they are closer to the upper limit, more electrons can be collected, i.e. higher collection efficiency. The value of the efficiency is the proportionality of the peak positions; one is the primary peak and the other is the characteristic peak of ^{55}Fe. In Fig. 4, the peak of the HR curve is closer to the characteristic peak than that of the NR curve, which can be explained by the HR's broader electric field. The collection efficiencies, as one of the most important factors of the MAPS, can be extracted by comparing the positions of the primary and characteristic peaks. In the simulations, the achieved values of collection efficiency are 73% in the NR structures and 88% in the HR ones, respectively. The corresponding results in experiments are 71% in NR and 91% in HR. Although there are some discrepancies in the results, it can be concluded that the simulated efficiency tends to be in agreement with the experiments.

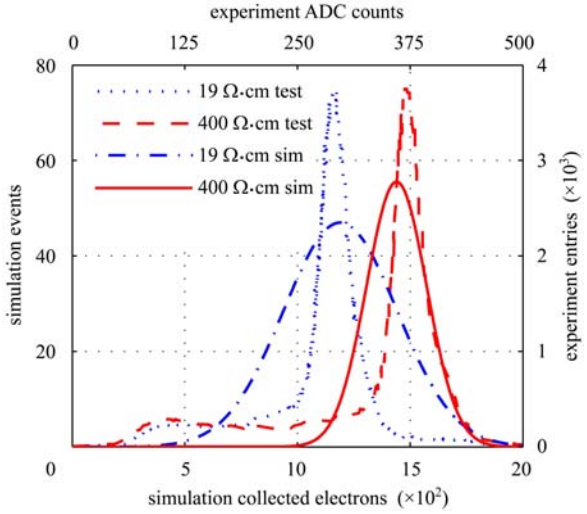

Fig. 4. Details of the charge collection efficiency of different epi-layers. The "test" and "sim" data come from real experiments and simulations, respectively. The experimental curves are labelled by the top-right axes and the others by the bottom-left ones.

3.2 Collection time

Because charge collection mostly depends on the location of ionizing incident radiation [8], four positions are selected to evaluate the collection time impartially. The first is sub-layer 01 cube 16, which is closest to o5; the second is sub-layer 05 cube 07 in the middle of the epi-layer; the third is sub-layer 06 cube 01, standing for the farthest position in the epi-layer; the last is sub-layer 10 cube 01, which can be regarded as the farthest one in the substrate. Due to the different distances from the strike position to the electrode, the collection time is reduced to varying degrees. As shown in Table 1, the difference in value of the first position is less than 10%. This is because the cube is near the N-well and all generated charges are in the collection electric field whether they are in HR or NR epi-layers. The second position is at the edge of the electric field in the HR pixels and there is no longer any electric field in the NR ones, which leads to more than a 50% reduction. Credit should be given to the broader and stronger field in the HR structures. With increasing distance, the reduction is lessened because the drift plays an increasingly weaker role in the electron transportation. Due to the randomness of X photon absorption in time and space, there seems no realistic method available to measure the collection time range accurately.

Table 1. Details of collection time, defined as when 90% of the total generated charges are collected by o5.

position	19/(Ω·cm)	400/(Ω·cm)	decrement
Sub-layer 01 cube 16	1.37 ns	1.24 ns	9.8 %
Sub-layer 05 cube 07	116.3 ns	52.8 ns	54.6 %
Sub-layer 06 cube 01	144.5 ns	74.4 ns	48.5 %
Sub-layer 10 cube 01	181.6 ns	122.8 ns	32.4 %

3.3 Neighboring diffusion

In Fig. 5, the percentage of the collected charges by each pixel is shown. The percentage of the seed point o5 increases from 34% to 43% when an HR epi-layer is used. In other pixels, the collected electrons are suppressed by about 1 or 2 percent. The charge diffusion among neighboring pixels is a negative effect for digital output MAPS because the collected charges in the seed point decrease and then lead to low signal-to-noise Ratio (SNR). In fact, the SNR at the seed pixel is improved from about 20 in the NR structure to 41 in the HR device, which can be observed in ^{106}Ru radiation experiments. It can be concluded that the simulations are in accord with the experiments.

Furthermore, if the diffusions can be suppressed, the fake hit rate and the spatial resolution are expected to improve [5].

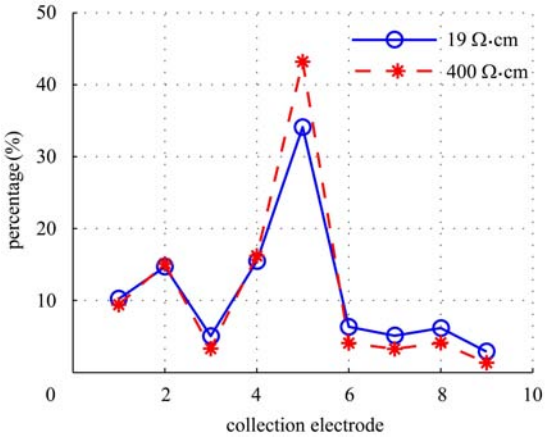

Fig. 5. Percentage of the collected electrons by each electrode.

4 Conclusion

This paper presents a novel simulation method to evaluate the charge collection performance of the MAPS detector. As a basis for the evaluation, 3×3 pixel matrix virtual devices with similar structures and different resistivity epi-layers are built with necessary physical models. Then, the virtual device is divided into hundreds of parts and an independent customized X photon model is involved in each part to simulate the conditions under ^{55}Fe radiation. Simulations at the physical level are carried out with the 3D oriented device simulator Sentaurus in transient mode. Detailed collection performances are established after data processing and the estimated values are compared with the experimental results obtained from the prototype MIMOSA-26 chips. The comparisons illustrate that the proposed idea is a feasible method to evaluate the MAPS collection performance, although there are some defects in the simulations.

There are several possible reasons for the differences between the simulation and the experiment. Firstly, the oxide belt used to consume the diffused electrons is a compromise approach, which would affect the electron movement in an undefined way. A bigger virtual device with more pixels would be a possible solution, but would require a powerful computer. Secondly, the modified X photon model does not completely accord with real ^{55}Fe radiation. The 6.4 keV photons and all other physical effects except ironing are neglected in the simulations and the initial distribution volume of generated charges is not a standard sphere. A more elaborate particle model using a segmented definition technique and a number of 6.4 keV photons should be applied. Finally, only just over a hundred events are involved in a roughly refined structure, but the absorbed X photons in the experiment are incalculable. A minutely meshed device structure and more particle events could be expected to cover the shortfall.

It is a pleasure to acknowledge Christine Hu-Guo, Andrei Dorokhov and Wojtec Dulinski from IPHC, France, who helped us in the early stage of this work.

References

1 Turchetta R et al. Nucl. Instrum. Methods Phys. Res. A, 2001, **458**: 677–689
2 Deptuch G et al. IEEE Trans. Nucl. Sci., 2002, **49**: 601–610
3 Heini S et al. IEEE Trans. Nucl. Sci., 2009, **56**: 346–353
4 Deptuch G, Dulinski W, Caccia M et al. IEEE Trans. Nucl. Sci., 2005, **52**: 1745–1754
5 Baudot J et al. First test results of MIMOSA-26, a fast CMOS sensor with integrated zero suppression and digitized output. In: IEEE Nucl. Sci. Symp. Conf. Rec., Orlando, US, 2009, 1169–1173
6 Battaglia M, Bussat J M, Contarato D et al. IEEE Trans. Nucl. Sci., 2008, **55**: 3746–3750
7 Dulinski W et al. IEEE Trans. Nucl. Sci., 2007, **54**: 284–289
8 Deptuch G et al. Nucl. Instrum. Methods Phys. Res. A, 2001, **465**: 92–100
9 Kennedy D P, O'Brien R P. IBM J. Res. Dev., 1969, **13**: 662–674
10 Buturla E M et al. IBM J. Res. Dev., 1981, **25**: 218–231
11 Pennicard D et al. IEEE Trans. Nucl. Sci., 2007, **54**: 1435–1443
12 Sentaurus User Guide, Synopsis Inc., 2008
13 Lund J, Olschner F, Bennett P et al. IEEE Trans. Nucl. Sci., 1995, **42**: 820–823
14 Husson D. Nucl. Instrum. Methods Phys. Res. A, 2001, **461**: 511–513
15 Fletcher N H. The high current limit for semiconductor junction devices. In: Proc. IRE., 1957, **45**: 862–872
16 Choo S C. IEEE Trans. Elec. Dev., 1972, **19**: 954–966
17 Huldt N G N L, Svantesson K G. Appl. Phys. Lett., 1979, **35**: 776–777
18 Lochmann W, Haug A. Solid State Commun., 1980, **35**: 553–556
19 Häcker R, Hangleiter A. J. Appl. Phys., 1994, **75**: 7570–7572
20 Selberherr S. Analysis and Simulation of Semiconductor Devices, Springer, 1984
21 Jain S C, Roulston D J. Solid-State Electron., 1991, **34**: 453–465
22 Deveaux M et al. Nucl. Instrum. Methods Phys. Res. A, 2003, **512**: 71–76